ACS Partner Journal

ACCOUNTS
—of materials research—

pubs.acs.org/amrcda

Article

Multiphysics Modeling Framework to Predict Process-Microstructure-Property Relationship in Fusion-Based Metal Additive Manufacturing

Wenda Tan* and Ashley Spear*

Cite This: *Acc. Mater. Res.* 2024, 5, 10–21

Read Online

ACCESS | Metrics & More | Article Recommendations

CONSPECTUS: Additive Manufacturing (AM) technology produces three-dimensional components in a layer-by-layer fashion and offers numerous advantages over conventional manufacturing processes. Driven by the growing needs of diverse industrial sectors, this technology has seen significant advances on both scientific and engineering fronts. Fusion-based processes are the mainstream techniques for AM of metallic materials. As the metals go through melting and solidification during the printing processes, the final microstructure and hence the properties of the printed components are highly sensitive to the printing conditions and can be very different from those of the feedstock. It is critical to understand the process-microstructure-property relationship for the accelerated optimization of the processing conditions and certification of the printed components. While experimentation has been used widely to acquire a mechanistic understanding of this subject matter, numerical modeling has become increasingly helpful in achieving the same purpose.

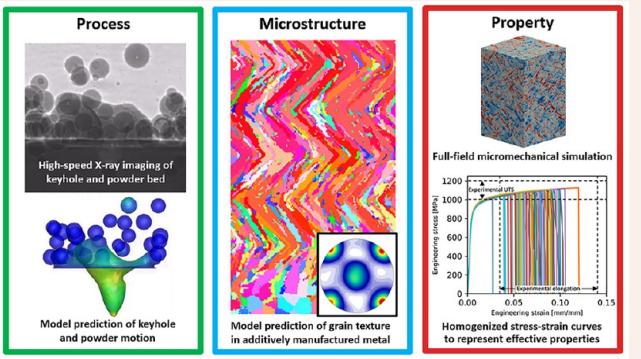

In this Account, the authors review their ongoing collaborative effort to establish a multiphysics modeling framework to predict the process-microstructure-property relationship in fusion-based metal AM processes. The framework includes three individual modules to simulate the dominating physics that dictate the process dynamics and microstructure evolution during printing as well as the responses of the printed microstructure to specific mechanical loadings. The process model uses the material properties and processing conditions as the inputs and simulates the laser-material interaction, multiphase thermo-fluid flow, and fluid-driven powder motion. It has successfully revealed the physical causes of depression zone shape variation as well as powder motion during the laser powder bed fusion process. The microstructure model uses the thermal history of the printing process and the material chemistry as the inputs and predicts the nucleation and growth of multiple grains in the multipass and multilayer printing processes. It has been used to understand the effects of inoculation and thermal conditions on grain texture evolution. The property models use microstructure data from simulations, experimental measurements, or statistical analyses as the inputs and leverage various computational tools to predict the mechanical response of the AM materials. These models have been used to quantitatively evaluate the effects of grain structure, residual strain, and pore and void defects on their properties and performance. While this and many other modeling works have significantly grown our collective knowledge of the process-microstructure-property relationship in fusion-based metal AM processes, efforts should be further invested in developing advanced theories and algorithms for the governing physics, leveraging data-driven approaches, accelerating simulation speed, and calibrating/validating models with controlled experimental measurements, among other aspects.

1. INTRODUCTION

Additive Manufacturing (AM) technology comprises a group of processes to join materials layer-by-layer to build three-dimensional (3D) components from computer-aided design (CAD) models. Fusion-based AM processes, viz., laser powder bed fusion (LPBF) and laser direct energy deposition (L-DED), are the mainstream technologies for metal AM. As the feedstock materials, usually in the form of powder or wire, are melted and solidified to print the geometries, the microstructure and properties of the products are highly dependent on the printing parameters and can differ dramatically from those of the initial feedstock. While great advancements have been achieved in understanding the process-microstructure-property (P-M-P)

Received: June 21, 2023
Revised: November 6, 2023
Accepted: December 16, 2023
Published: January 12, 2024

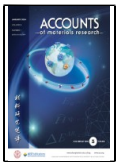

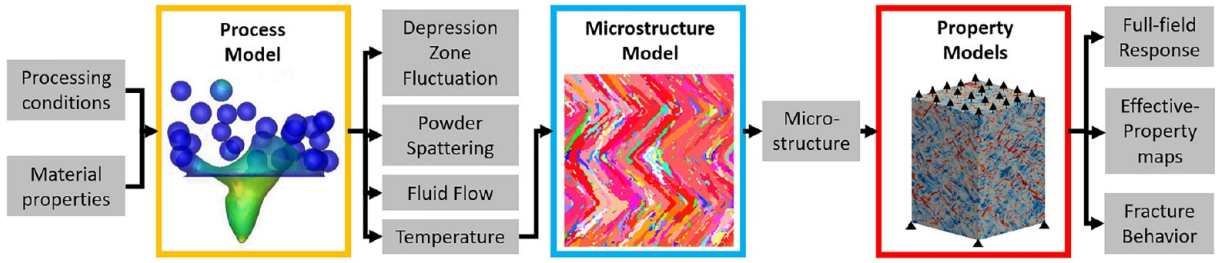

Figure 1. Overall flowchart of modeling framework for fusion-based metal Additive Manufacturing (AM). "Process Model" block shows simulated depression zone shape and powder motion in laser powder bed fusion. "Microstructure Model" block shows a simulated grain structure for a multilayer build. "Property Models" block shows a micromechanical simulation of an AM microstructure with applied loading. Relevant inputs and outputs to each model are depicted in shaded boxes.

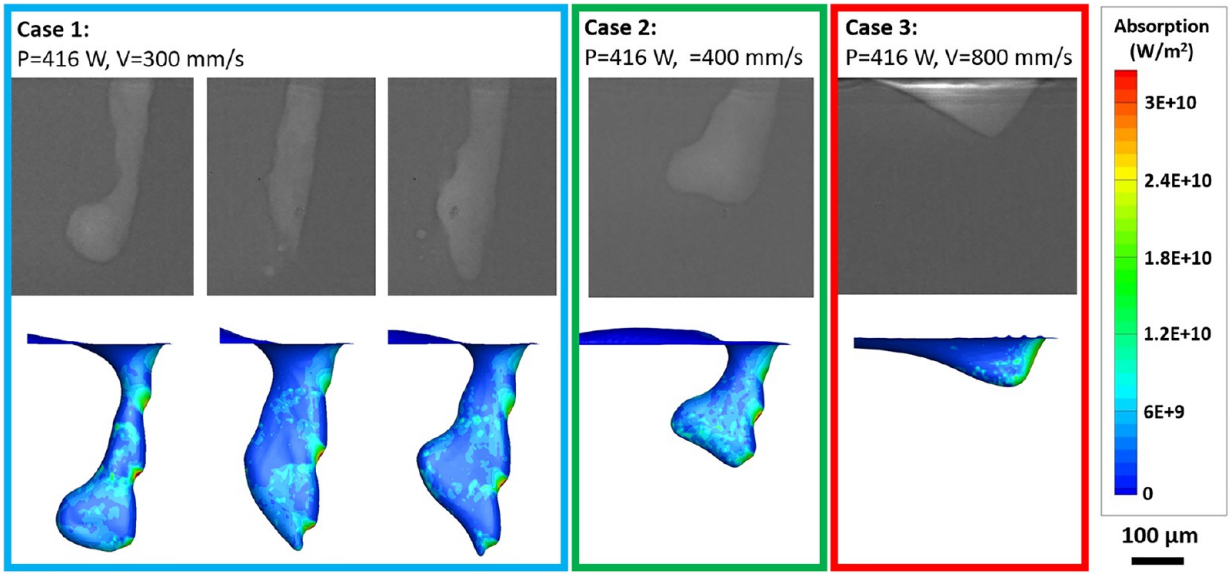

Figure 2. Comparison of depression zone shapes from dynamic X-ray imaging (top row) and computational physics model (bottom row) for three cases. Three different snapshots are given for case 1 to demonstrate depression zone fluctuation. Only one snapshot is given for cases 2 and 3 because depression zone is relatively stable. Depression zone in simulation results is colored by the intensity of laser absorption.

relationships, it is still difficult and expensive to optimize the process and quantify uncertainties in the resultant microstructure and properties when a new material or a new geometry is printed.

Experimental methodologies are frequently utilized to garner insight into this topic, but fusion-based AM processes present some unique challenges for experiments. The processes involve high temperatures above the melting/boiling points of the metals, significant variances in temperature and flow velocity occur across several hundred micrometers within microseconds, and the resulting microstructures often possess critical features at the micrometer/nanometer scale. Furthermore, these quantities are buried within the domain and are difficult to measure from the exterior. Given the limitations of current technologies, achieving the necessary spatial and temporal resolutions for many of these quantities is either expensive or even unfeasible.

Computational modeling, by solving appropriate governing equations to capture the relevant physics, can provide quantitative predictions of the physical terms at any moment and location. It complements experimental approaches and plays an indispensable role in acquiring a complete understanding of the P-M-P relationships in metal AM. There have been multiple salient literature reviews for AM modeling,[1−3] and this accounts article is instead intended to describe the authors' experience and perspectives regarding this topic.

The Laboratory of Computational Manufacturing at the University of Michigan (previously located at the University of Utah) and directed by Dr. Wenda Tan, and the Multiscale Mechanics and Materials Laboratory, located at the University of Utah and directed by Dr. Ashley Spear, have been collaborating to establish a multiphysics modeling framework to predict the P-M-P relationship for fusion-based metal AM processes (see Figure 1). The processing conditions and materials properties are fed into the process model to simulate the physical phenomena in and around the molten pool. The model generates thermal histories of the printing processes and feeds them into the microstructure model, which simulates the nucleation and growth of all grains during molten pool solidification and ultimately predicts the final grain texture within the printed materials. This is fed into the property models to simulate the responses of the printed materials under certain mechanical loadings. In this Account, the basic modeling approaches and typical results of the three models are reviewed.

2. PROCESS DYNAMICS MODELING

In fusion-based metal AM, the process dynamics are governed by the interplay of multiple physics, including energy absorption,

https://doi.org/10.1021/accountsmr.3c00108
Acc. Mater. Res. 2024, 5, 10−21

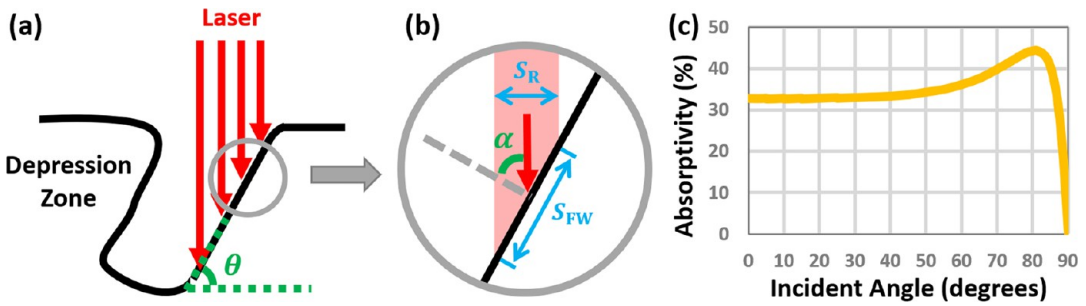

Figure 3. Laser absorption on front wall of depression zone. (a) Definition for inclination angle θ of front wall. (b) Definition for incident angle α of a laser ray on front wall and demonstration of spread of this laser ray of size S_R to an area of S_{FW} on inclined front wall. (c) Variation of laser absorptivity as a function of incident angle according to Fresnel equation.

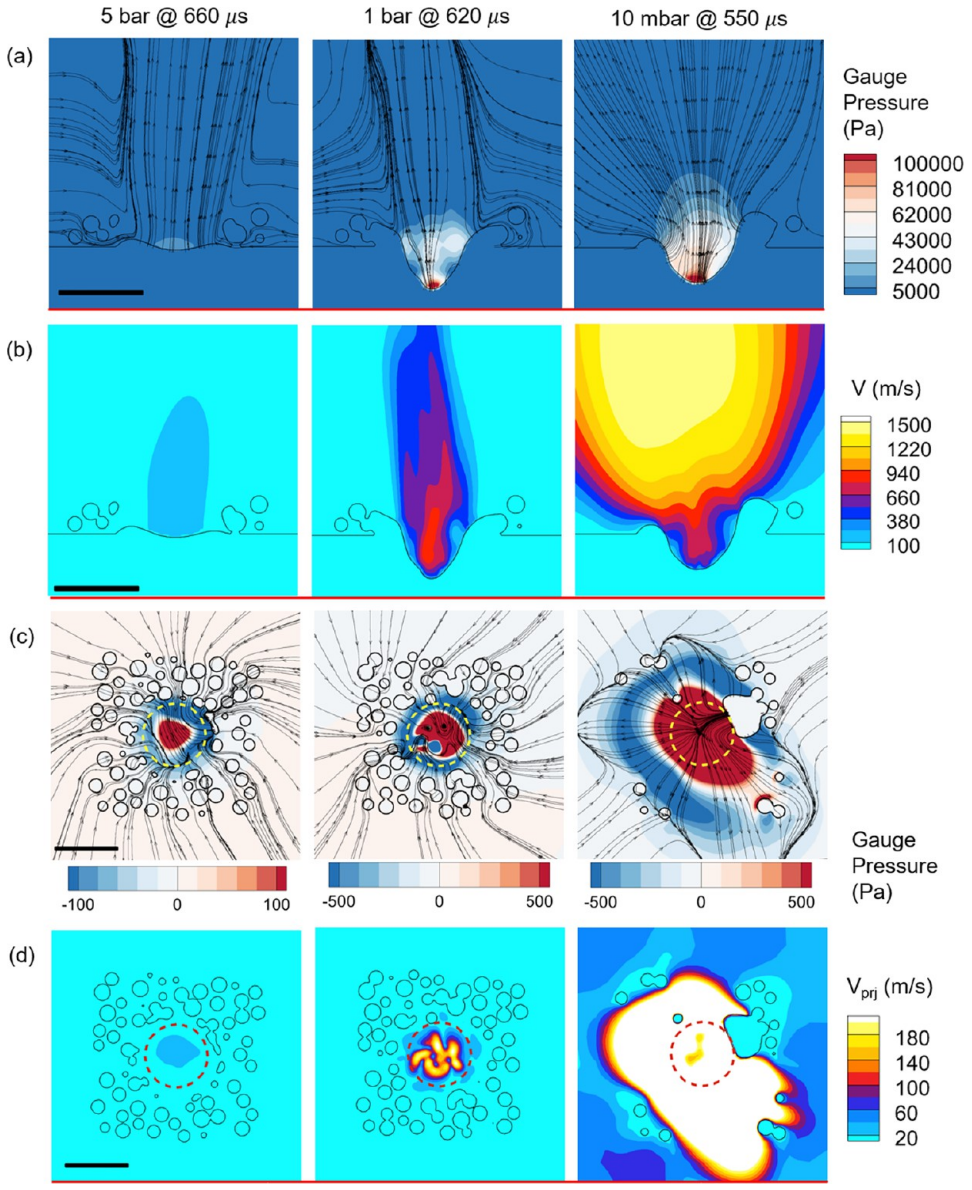

Figure 4. Gas flow structure at quasi-steady state for cases of different ambient pressure (5 bar, 1 bar, and 10 mbar). (a) Gauge pressure and streamlines on vertical plane at laser beam center, and (b) velocity magnitude. (c) Gauge pressure and streamline on a horizontal plane cutting through powder bed, and (d) velocity magnitude. Dashed circles in (c) and (d) indicate laser illumination zone. All scale bars are 200 μm.

phase change, multiphase heat transfer and fluid flow, dynamic interface movement, and fluid-particle interaction. These physics collaborate to cause complex, and sometimes unstable, process dynamics, which are considered a major contributor to multiple quality-critical phenomena, e.g., pore formation and powder denudation/ejection.

https://doi.org/10.1021/accountsmr.3c00108
Acc. Mater. Res. 2024, 5, 10−21

Tan's lab has been working on a computational physics model to simulate the process dynamics for fusion-based AM processes.[4−8] This model includes (i) a ray-tracing subroutine to predict the laser absorption by the metal surface; (ii) a computational fluid dynamics (CFD) subroutine to simulate the thermo-fluid flow in gas (environmental gas and metal vapor), liquid (molten pool), and solid (substrate and unmelted powder); (iii) a Level-Set subroutine to capture the movement of molten pool surface; and (iv) a discrete element subroutine to capture the particle motion driven by gas-particle and particle−particle interaction. It has been calibrated and validated for multiple engineering materials by comparing the modeling predictions with the in situ X-ray imaging of depression zone geometry and ex situ optical imaging of the molten pool cross-section shape. The simulation results provided insight into the depression zone behavior and powder motion in LPBF.

2.1. Behavior of Depression Zone

In LPBF, metal evaporation can be induced by laser heating and generates recoil pressure on the molten pool surface that creates a depression zone. Experiments have shown that the shape of the depression zone can change significantly by the variation of process parameters, particularly laser power and scanning speed.[9] The computational physics model has reproduced the different depression zone shapes (see Figure 2) and provided physical explanations.[6]

A higher laser power generates a higher recoil pressure, and a lower scanning speed allows the laser to dwell in a region so that the recoil pressure can accelerate the liquid flow for a longer time. Both lead to a higher drilling velocity and hence a large inclination angle θ (defined in Figure 3a) for the Front Wall (FW) of the depression zone. As θ increases, the incident angle α (defined in Figure 3b) of the laser on the FW becomes larger, and the laser absorptivity changes according to the Fresnel equation (as plotted in Figure 3c). Furthermore, any laser ray with an initial size of S_R illuminates an area of S_{FW} on the FW (as shown in Figure 3b). S_{FW} becomes larger as θ increases, which effectively decreases the power density of laser absorption on the FW. Therefore, the FW temperature decreases, and the evaporation is reduced. A lower recoil pressure is available, and thus the large inclination of the FW becomes difficult to maintain. To still maintain a large FW inclination, protrusions need to form on the FW. The upper side of the protrusions can effectively obtain a high density of laser absorption, which induces intensive local evaporation and hence strong recoil pressure. The recoil pressure pushes the protrusions to move downward rapidly, which keeps the FW at a large inclination angle. The downward motion of these protrusions, however, introduces instabilities into the system. Each protrusion generates a wave of rapid flow that propagates across the molten pool and can potentially alter the depression zone shape. If the shape change is too severe, the depression zone can collapse occasionally, generating bubbles in the molten pool that can ultimately become pores in the final part.

In the opposite cases with a lower laser power and/or a higher scanning speed, the FW is less inclined. The incident angle of the laser on the FW is smaller than the Brewster's angle, and the laser absorptivity becomes less sensitive to the incident angle. This significantly reduces the spatial variation of laser absorption on the FW of the depression zone, where protrusions, even if formed, cannot survive. As the FW is stabilized in these cases, the entire depression zone experiences fewer fluctuations.

2.2. Gas Flow and Powder Motion

Another outcome of laser-induced evaporation is a high-speed and high-temperature vapor jet, which drives the environmental gas to flow. The flow of the metal vapor and environmental gas drives the powder motion (e.g., denudation and ejection), which can lead to a series of deleterious features in the final builds. The computational physics model in Tan's lab can reveal the gas flow structure and the gas-driven particle motion.

Simulations were performed for LPBF cases with a stationary pulse laser and different ambient pressure levels,[7,8] and a consistent gas flow pattern was observed in all cases. Metal vapor was generated at the bottom of the depression zone due to laser-induced metal evaporation. Driven by the large pressure gradient from the bottom of the depression zone to its opening (Figure 4a), the metal vapor flux developed into a high-speed jet (Figure 4b). A low-pressure ring was generated around the vapor jet, right above the substrate (Figure 4c). The pressure gradient from the ambient to the low-pressure ring induced an entrainment flow that drove the ambient gas to flow toward the vapor jet (Figure 4d).

As the ambient pressure varied from hyper-atmospheric (5 bar, first column in Figure 4) to atmospheric (1 bar, second column in Figure 4) and then to hypo-atmospheric (10 mbar, third column in Figure 4) levels, the vapor jet velocity increased from 200 to 1500 m/s, the entrainment flow velocity increased from 5 to 50 m/s, the divergent angle of vapor jet significantly increased, the vapor jet temperature decreased from 3400 to 2100 K, and the Knudsen number (Kn) of the gas flow increased from the range ($0.0004 \sim 0.004$) to ($0.05 \sim 0.5$). Note that the continuum assumption of the gas flow may break down when the ambient pressure is below 10 mbar ($Kn \gtrsim 0.2$).

The simulations also revealed the interactions between the gas flow and powder particles that drive the powder motion. Four characteristic modes of powder-gas interaction were identified according to the dominating physics and the total force direction of the powder particles.

- Recoil mode is defined when significant evaporation occurs on the powder particle surface, and the recoil pressure dominates over the drag force of the gas flow on the particle surface. The powder particle is driven away by the vapor jet generated by the evaporation on the particle surface.
- Entrainment mode is defined when the particle is surrounded by the entrainment flow. The particle is driven by the drag force of the entrainment flow and moves toward the laser illumination zone.
- Expulsion mode is defined when the particle is surrounded by the expanding vapor jet. The particle is ejected by the drag force of the vapor jet with a relatively large divergence angle.
- Elevation mode is defined when the particle is simultaneously subject to the entrainment flow and the vapor jet expansion. The simultaneous effects of the two flows drive the particle to move upward with a relatively small divergence angle.

These four interaction modes, individually or collectively, control the motion of each particle. Sometimes one mode dominates the entire particle trajectories and sometimes several modes sequentially dominate the particle trajectories.

https://doi.org/10.1021/accountsmr.3c00108
Acc. Mater. Res. 2024, 5, 10−21

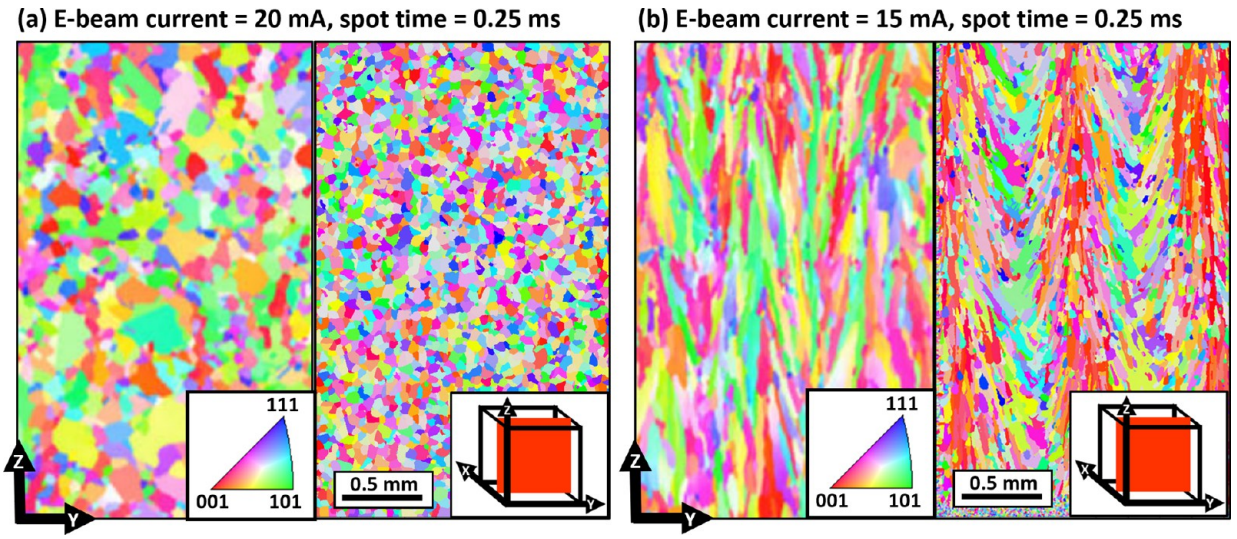

Figure 5. Grain texture of two cases in electron-beam additive manufacturing of Inconel 718 alloy. Left insets show experimental results obtained from electron backscatter diffraction characterization, and right insets show simulation results obtained from Cellular Automata model.

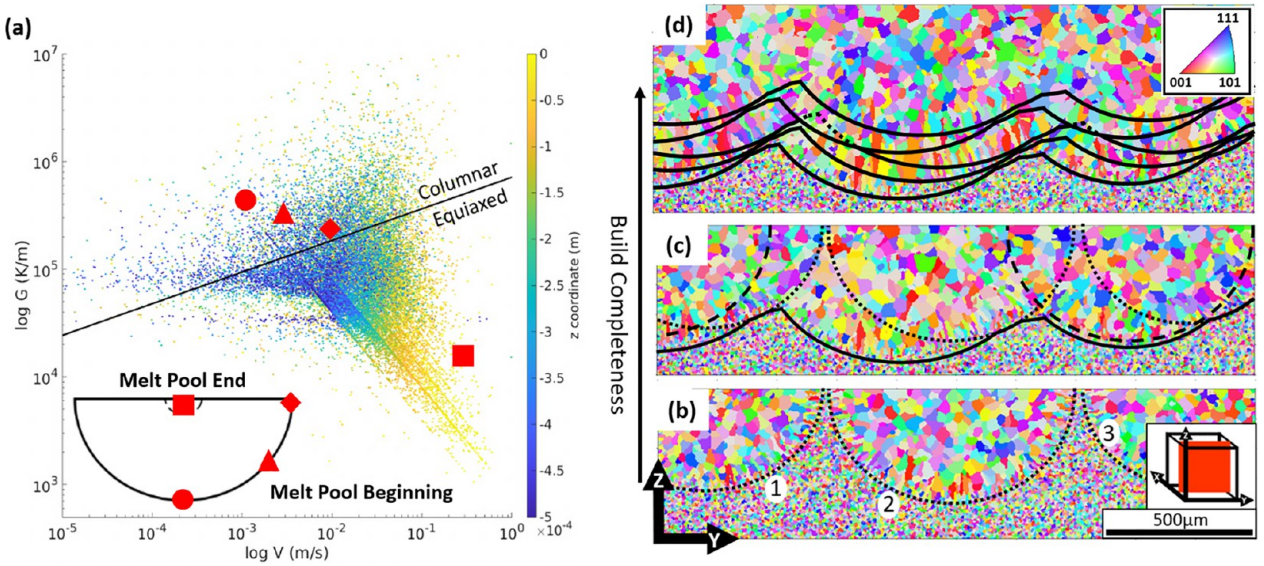

Figure 6. Explanation of thermal conditions and grain texture evolution in electron-beam additive manufacturing of Inconel 718. (a) Distribution of thermal conditions for molten pool solidification, with inset showing locations of selected points in molten pool. Points were colored by their vertical coordinates, with zero coordinate indicating top surface and negative values indicating locations beneath top surface. (b) First three molten pools in first layer, with columnar-to-equiaxed transition occurring in each molten pool. (c) Locations of all molten pools and final grain texture after one layer. (d) Fusion lines of five layers and grain texture after five layers.

3. GRAIN STRUCTURE MODELING

In fusion-based metal AM processes, the feedstock materials are deposited, remelted, and solidified on the top of the printed components. The grain texture, dictated by the size and crystallographic orientation of all grains in the domain, is determined by the collaboration of the material properties and processing conditions. It is critical to control the grain texture, which poses decisive influences on the final properties of the AM parts.

In Tan's lab, a 3D Cellular Automata (CA) model has been developed to simulate grain growth during fusion-based metal AM processes.[10,11] The model takes 3D thermal histories from a process model as the input, uses certain analytical models for dendrite growth (e.g., KGT model[12]) to calculate the grain growth kinetics (i.e., the grain growth velocity as a function of the material composition and local temperature), and utilizes a decentered square algorithm to explicitly track the envelope expansion of each grain during its growth. The solute redistribution and subgrain dendritic growth within the grains were not explicitly simulated in this model but were implicitly considered in the analytical model for the growth kinetics calculation. An additional algorithm is included to simulate the heterogeneous nucleation with which new nucleation sites appear in the molten pool to initiate the growth of new grains of arbitrary crystallographic orientations. Ultimately, the model can simulate the growth and remelting of all grains during the complex thermal histories of the printing processes and predict the final grain texture in the final parts. The model has been validated by comparing the predicted grain textures with the Electron Backscatter Diffraction (EBSD) characterization results for cases of different processing conditions and

https://doi.org/10.1021/accountsmr.3c00108
Acc. Mater. Res. 2024, 5, 10−21

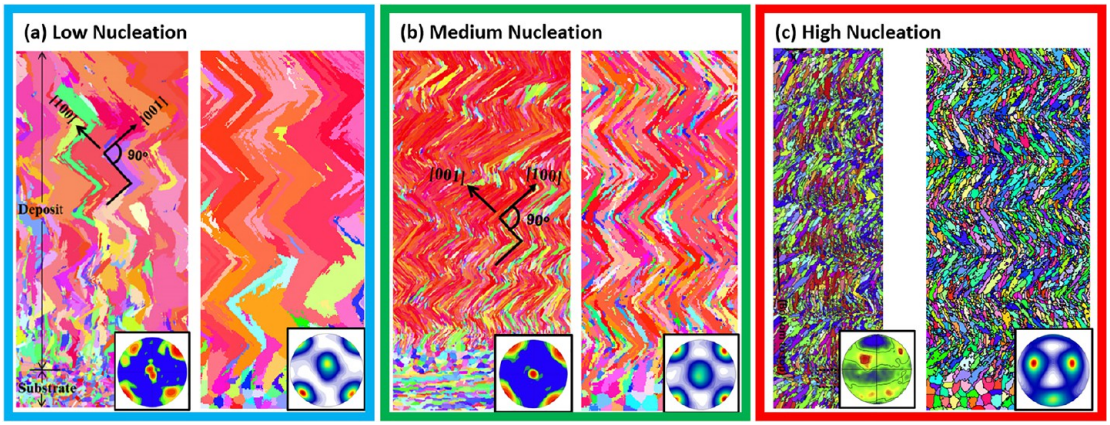

Figure 7. Grain textures with different nucleation frequencies. In each case, left inset shows experimental results of electron backscatter diffraction (EBSD) characterization, and right inset shows simulation results from Cellular Automata model.

engineering materials and has been used to investigate the effects of the processing conditions and the nucleation events on the final grain texture in metal AM builds.

3.1. Effects of Processing Conditions

Abundant experiments have demonstrated grain texture to be highly dependent on processing parameters, including but not limited to the heat source power and scanning speed, hatch spacing, and scanning pattern. The CA model offers a feasible approach to understanding grain texture evolution during the printing processes with different parameters.

In collaboration with Oak Ridge National Laboratory, Tan's lab applied the CA model to investigate the grain texture evolution as a function of processing conditions for the Electron-Beam Additive Manufacturing (EBAM) of Inconel 718.[10] In that work, a complex scanning strategy was used. In each layer, a series of spot heatings was applied on the powder bed according to a specific sequence. This spot-heating sequence was applied to every layer with a shift within the build plane between consecutive layers.

Different electron beam (e-beam) currents and spot times were used in different cases, producing significant variations in thermal histories and, hence, grain textures. In the case with long e-beam spot time and high e-beam current values, the molten pool created by each spot heating was larger in size and survived longer in time, so all of the molten pools in the later stage of each layer were connected to produce one integrated molten pool. The temperature gradient (denoted as G) of this integrated molten pool was relatively low during its solidification, which encouraged the formation of equal grains throughout each layer. As a result, the entire build was dominated by equiaxed grains (see Figure 5a). In the cases with short e-beam spot time or low e-beam current values, the grain texture was dominated by columnar grains (Figure 5b), but the grain texture evolution was found to be more complicated.

Due to the lower e-beam energy input at each spot, each molten pool was relatively small and separate from other molten pools. In every molten pool, the early stage of its solidification took place near the fusion zone edge (e.g., at the diamond, triangle, and circle positions in Figure 6a). The local G was high enough to encourage the growth of columnar grains (Figure 6b). In the later stage of the molten pool solidification, the solidification front moved to the fusion zone center (e.g., at the square location in Figure 6a). The local G became relatively low and encouraged the growth of equal grains (see Figure 6b). The columnar-to-equiaxed transition (CET) occurred during the solidification of all molten pools. As multiple molten pools occurred sequentially in each layer, the final grain texture at the end of each layer was predominantly columnar on the bottom and equiaxed at the top (Figure 6c). But the equiaxed grains did not survive in the final parts as they were completely remelted by the next layers. Only the columnar grains located at the bottom of the layer remained (see Figure 6d), and as a result, only columnar grains survived in the final grain texture (see Figure 5b).

3.2. Effects of Nucleation

Nucleation during metal solidification in metal AM has been found to significantly alter the grain structure and hence the properties of the products,[13] but the effects of nucleation had not been previously understood from a quantitative standpoint. Tan's group performed a parametric study using the CA model to investigate this matter.[11]

In that work, nucleation was treated as a stochastic event dictated by the nucleation density (denoted as N_0) and the critical nucleation undercooling (denoted as ΔT_c), both of which were material dependent. Parametric simulations of varying nucleation parameters were performed with the CA model. The nucleation events became more frequent by increasing N_0 or decreasing ΔT_c, and the model predicted very different grain textures, all of which were found to well resemble experimental results.

- In the case of rare nucleation events (see Figure 7a), every layer was dominated by columnar grains, all of which continued to grow in the following layers and competed with each other along the building direction. Competitive growth existed throughout the entire build, and only several grains survived the competition. They dominated the entire domain, with each being very large in size.
- In the case of a moderate number of nucleation events (Figure 7b), some new equiaxed grains appeared (primarily in the top portion of the molten pool) due to the nucleation events and they mixed with the columnar grains in each layer. When the next layer was printed, it remelted the top portion of the previous layer. The partially melted grains on the fusion line, either columnar or equiaxed ones, grew to become columnar grains in the next layer. As this process repeated in every layer, equiaxed grains were introduced as the new "competitors" in the competitive growth, and it became almost

https://doi.org/10.1021/accountsmr.3c00108
Acc. Mater. Res. 2024, 5, 10−21

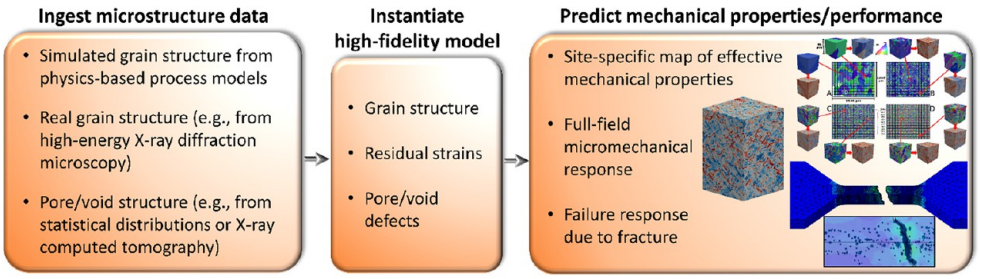

Figure 8. Microstructure−property modeling workflow comprising codes for ingesting microstructural data from various sources, instantiating high-fidelity models, and simulating mechanical response for applications in metal additive manufacturing.

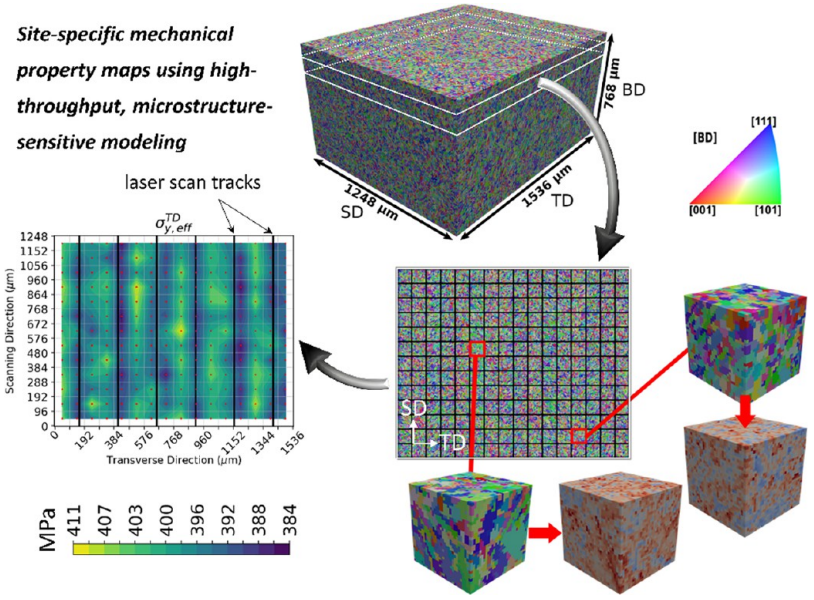

Figure 9. Automated workflow for ingesting microstructure from physics-based models, performing high-throughput micromechanical simulations, and generating maps of effective (homogenized) mechanical properties for metal additive manufacturing.

impossible for a few grains to outgrow all other grains. Therefore, a large number of grains existed in the final structures, all presenting small sizes and needle-like shapes.

- In the case of excessive nucleation events (see Figure 7c), CET occurred in each layer and the top portion of each layer was completely occupied by equiaxed grains. When the next layer was printed, only a portion of the "equiaxed region" in the previous layer was remelted, and the partially remelted equiaxed grains grew to become the columnar grains in the next layer. As this pattern repeated layer upon another, the columnar and equiaxed layers formed alternatively.

4. MECHANICAL RESPONSE MODELING

In general, the bulk mechanical response of a polycrystalline material is governed by anisotropic deformation mechanisms that act across length scales. Accounting for the combination of intrinsic deformation mechanisms (e.g., crystallographic slip and twinning), microstructural heterogeneities, and complex neighbor-neighbor interactions among microstructural features presents a unique challenge for accurately modeling micromechanical behavior of polycrystalline metals.[14] In metals produced via AM, this modeling challenge is exacerbated[15−17] due to the presence of residual strains and pore or void defects, which can significantly modify the mechanical properties and performance of structural components.

In Spear's lab, a suite of microstructure−property models has been integrated into a modular workflow in which microstructural features are represented with high-fidelity (viz., with respect to current 3D materials imaging resolution limits) to capture their influence on the mechanical properties of AM metals. Modularity enables the microstructure data from different sources to be leveraged. As shown in Figure 8, microstructure data can be ingested from the physics-based process models presented above, from experimental measurements (e.g., high-energy X-ray diffraction microscopy or X-ray computed tomography), or from statistical measures of microstructural features. The ingested data are used to instantiate a model in which the features of interest (grains, residual strains, and pore and void defects) are represented with high fidelity. Subsequently, the high-fidelity model is passed to an appropriate numerical solver capable of modeling the mechanical response of interest. Within this framework, Spear's group has developed, adopted, and augmented various computational tools to address some of the unique challenges associated with predicting the structure−property linkages in metal AM. Several case studies are presented below to illustrate the range of predictions to date.

https://doi.org/10.1021/accountsmr.3c00108
Acc. Mater. Res. 2024, 5, 10−21

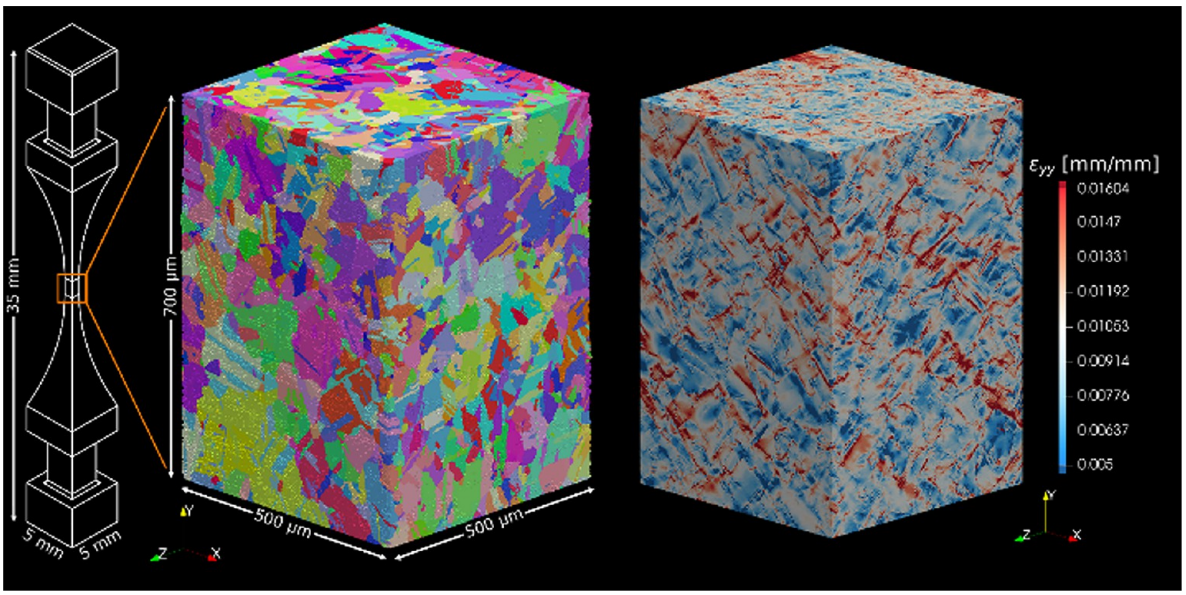

Figure 10. Tensile specimen with magnified view of experimentally characterized microstructure of IN625 manufactured by laser powder bed fusion for the AFRL AM Modeling Challenge.[24,25] At right is the predicted axial strain field from micromechanical modeling.[23]

4.1. Site-Specific Maps of Effective Mechanical Properties

Due to the variation of thermal conditions in the printing process, the final grain texture can be significantly different from one location to another within a single part. The effective (homogenized) mechanical properties, therefore, can also vary spatially throughout a given build domain. A convenient way to assess the spatial variability of effective mechanical properties is by generating property maps, analogous to those generated in 2D from indentation tests (e.g., see ref 18). Two challenges with mapping the effective mechanical properties throughout an entire AM build domain are (1) the effective mechanical properties inherently depend upon the 3D grain structure, such that the latter must be explicitly modeled to obtain accurate mechanical-property predictions, and (2) meeting the first challenge is computationally expensive and can become intractable depending on the numerical solver employed and the size of the AM build domain (hence, simulation domain size).

Spear's lab recently implemented an automated workflow that integrates with Tan's microstructure-prediction framework and addresses the aforementioned challenges to provide site-specific maps of effective mechanical properties in AM metals. Succinctly put, the workflow ingests the grain-resolved build domain from the microstructure simulations in section 3, divides the build domain into subvolumes of a user-specified size, prepares and passes a data file for each microstructural subvolume to an elasto-viscoplastic Fast Fourier transform (EVPFFT) code, simulates mechanical loading for each microstructural subvolume, retrieves and postprocesses the results, and plots the results as a heat map of effective mechanical properties.

The key to generating the spatial property maps using high-fidelity microstructural modeling is the integration of a parallelized version of the EVPFFT code, called MASSIF,[19] into the automated workflow to enable *high-throughput virtual mechanical testing* of microstructural subvolumes. As an example, the workflow was used to generate maps of effective yield strength throughout four distinct build domains of L-DED stainless steel 316L by performing 7680 microstructure-sensitive numerical simulations (each to 1% total strain, well beyond macroscopic yielding).[20] Figure 9 shows a property map in a single layer of one of the AM builds. The MASSIF code was originally implemented by Rollett[19] and is based on the EVPFFT formulation by Lebensohn.[21] Spear's group adopted the MASSIF code and augmented it to account for grain-boundary strengthening by implementing a scaling relationship between the initial critical resolved shear stress (τ_0) and the slip-directed-distance to nearest grain boundary. The slip-directed distance is defined as the distance parallel to the Burgers vector from a given point in the simulation domain to the nearest grain boundary; thus, a unique τ_0 is defined for each slip system at each point in the simulation volume. A composition-dependent solid-solution strengthening model is not currently included in the model, and its future incorporation could serve to further improve the constitutive representation in the EVPFFT code.

The ability to estimate effective, microstructure-dependent mechanical properties, throughout entire AM build domains has important implications for the design and qualification of metal AM. For example, the property maps can be used to assess the degree of effective anisotropy, spatial variability from expected nominal properties, and prevalence of "hot spots" throughout a given build, enabling design engineers to determine whether a particular build meets quality assurance metrics for structural applications. From a scientific standpoint, the maps also provide new insight into the relationship between the building process and the distribution of mechanical properties. For example, the map of effective yield strength in the transverse direction ($\sigma_{y,eff}^{TD}$) for the particular L-DED build domain and layer depicted in Figure 9 exhibits a banding pattern aligned with the laser scan tracks, where $\sigma_{y,eff}^{TD}$ is generally lower along the scan tracks and higher in between scan tracks. The integrated multiphysics modeling framework was able to reveal this unique phenomenon, which is fundamentally related to the simulated thermal history and microstructural evolution for the multipass, multilayer L-DED process.

https://doi.org/10.1021/accountsmr.3c00108
Acc. Mater. Res. 2024, 5, 10−21

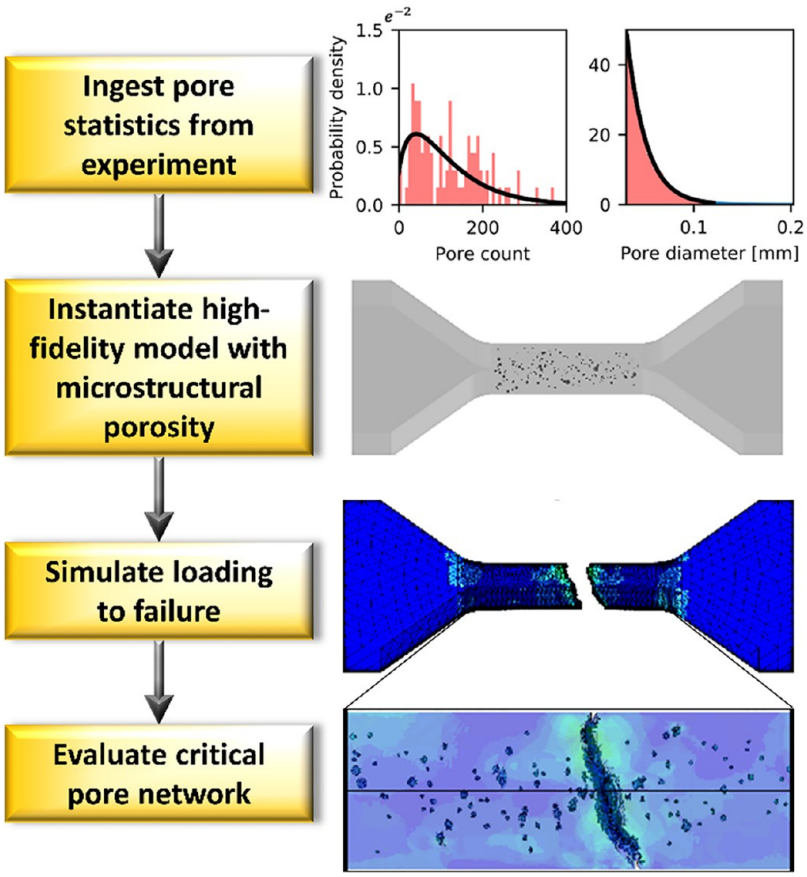

Figure 11. Automated workflow for instantiating high-fidelity models with microstructure porosity to evaluate its effect on the failure of AM metal.

4.2. Full-Field Micromechanical Response Accounting for Residual Strains

It has been well documented that laser-based AM processes can induce non-negligible residual stresses, which can lead to part distortion and impact mechanical performance of the final part.[22] Depending on the severity of the residual stress, postbuild heat treatments can be applied, and identifying optimal heat treatments for specific build parameters and materials remains the topic of ongoing research in the community.

Spear and collaborators recently leveraged the microstructure−property workflow depicted in Figure 8 to assess approaches for incorporating residual strains into the EVPFFT modeling framework and the relative impact of each approach on micromechanical predictions.[23] The investigation was performed within the context of the Air Force Research Laboratory (AFRL) AM Modeling Challenge Series. Specifically, Challenge Problem 4 in the Series solicited participants to make blind predictions of grain-averaged strain tensors in 28 challenge grains at six specific stress states given a 3D microstructural image of a tensile specimen and its corresponding macroscale engineering stress−strain response.[24,25] The tensile specimen was produced using LPBF with IN625 powder. The microstructure data and grain-averaged elastic strains provided by AFRL were experimentally characterized with high-energy X-ray diffraction microscopy (HEDM) during an in situ tensile test performed at the Advanced Photon Source 1-ID-E beamline at Argonne National Laboratory.[26−29] Given the time constraints of the challenge, Spear's team neglected residual strains in the EVPFFT model used for challenge submission. Nonetheless, among all submissions, the EVPFFT-based predictions submitted by her team achieved the lowest total error in comparison to experimental results and received the award for Top Performer. Figure 10 depicts the AM IN625 microstructure and simulated strain field.

Spear's team performed a postchallenge investigation to assess improvement relative to the submitted predictions by incorporating initial elastic strains. Of the five approaches considered for incorporating initial elastic strains, all outperformed the model in which initial elastic strains were neglected. However, the best predictions were achieved by initializing an eigenstrain field[30] using an Eshelby approximation,[31] which, for the first time in the context of EVPFFT modeling, was carried out using an ellipsoidal grain-shape approximation. The method for calculating the eigenstrain field from the initial elastic strain field was subsequently incorporated into the open-source software DREAM.3D.[32]

The findings from this case study provide a quantitative assessment of the impact of residual strains on the micromechanical (grain-scale) response of an AM metal. In this example of the microstructure−property workflow, the ingested microstructure data were derived from experiment, and a high-fidelity model was instantiated to include both the grain structure and experimentally measured residual strains. With this experimentally validated approach as a backdrop, future micromechanical models will be seamlessly integrated with Tan's framework to instantiate models with residual strain fields from physics-based process modeling.

4.3. Failure Response Due to Void Defect-Induced Fracture

Pore and void defects caused by keyholing, lack of fusion, and gas porosity are common outcomes of the AM process and

https://doi.org/10.1021/accountsmr.3c00108
Acc. Mater. Res. 2024, 5, 10−21

exhibit varying degrees of severity depending upon processing parameters.[33] These microstructural defects can significantly change the mechanical performance of AM parts[34] and should therefore be considered when modeling structures for use in fracture-critical applications.

Following the workflows depicted in Figures 8 and 11, Spear's lab assessed critical characteristics of pore networks that impact fracture behavior in AM metals by implementing an approach for automatically instantiating models with realistic pore structures and simulating loading to failure.[35] Based on experimentally derived pore data in AM 17-4PH stainless steel produced by LPBF,[36] distributions of pore count and pore diameter were created and sampled to generate 120 unique realizations of pore structures in the gauge section of a standard tensile specimen. The models were then analyzed by using the finite-element method. Based on findings from the Third Sandia Fracture Challenge,[37,38] Spear's group leveraged an element-deletion approach to simulate material degradation and failure of the specimens, and mechanical properties (e.g., yield and ultimate strengths, ductility, and toughness modulus) were recorded. Subsequently, a correlation analysis was performed between the mechanical properties and commonly reported pore metrics (e.g., volume fraction porosity, maximum pore diameter, and maximum and average cross-section-area reduction). Additionally, a new metric, called the void descriptor function (VDF), was derived to characterize pore networks by accounting for the pore size, pore clustering, and pore position relative to free surfaces. The VDF metric was found to have stronger correlations with post-yield mechanical properties than did all other pore metrics that were considered. Furthermore, the location of the maximum VDF was found to serve as a good indicator of fracture location. More recently, the VDF was modified to account for neighbor-neighbor interactions and stress concentrations associated with nonspherical pores, and the modified VDF was experimentally evaluated by comparing to tensile test results for AM IN718 mesoscale specimens produced by LPBF.[39]

The ability to simulate failure response by accounting explicitly for microstructural porosity and void defects has important implications for structural prognosis and reliability assessment of AM metal parts. Furthermore, a significant outcome from this work—enabled by the high-fidelity representation of pore structures—is the derivation of the VDF as a novel descriptor of pore networks, which could be incorporated into a screening tool to aid in predicting, *a priori*, likely locations of fracture and post-yield mechanical properties.

5. CONCLUSIONS, CHALLENGES, AND PERSPECTIVES

This Account presents a summary of an ongoing effort to develop a physics-based modeling framework to predict the P-M-P relationship for fusion-based metal AM processes.

- A computational physics model has been developed to simulate the complex physics for depression zone, molten pool, and powder particles during the process, and it can reproduce the typical phenomena observed in experiments. The simulations have helped to understand the causes of different shapes of depression zone and its fluctuation. The simulations have also quantitatively revealed the gas flow structure in LPBF and the gas-powder interaction that drives the powder motion.
- A computational materials model based on the Cellular Automata method has been developed to predict the complex grain structures in AM parts. The model has demonstrated the grain structure evolution during different complex thermal histories generated by different processing conditions. It has also disclosed the effects of heterogeneous nucleation on the grain texture development.
- A modular microstructure—property workflow has been presented, in which microstructural features of interest are explicitly modeled with high fidelity to capture their effect on resulting mechanical behavior. For cases in which high-throughput micromechanical responses are desired to predict, for example, the spatial variability of effective mechanical properties throughout an entire 3D build domain, a parallelized EVPFFT code has been adopted and integrated into an automated pipeline to generate mechanical-property maps, accounting for grain-boundary strengthening. For cases in which unique pore networks and fracture behavior are of interest, a finite-element-based framework has been adopted and integrated into an automated pipeline to predict distributions of failure response. Besides enabling predictions that are relevant for the certification and qualification of AM parts, the framework enables scientific discoveries relating the AM process to mechanical properties via explicit treatment of the microstructure.

While this modeling framework and many other modeling efforts in the community have already significantly grown our collective knowledge for fusion-based metal AM processes, challenges remain for the entire AM modeling community to further improve our understanding.

- Theories and algorithms should be honed as our collective understanding of the governing physics is improved. For example, process models need improved theories to capture the interaction between laser and the vapor plume. Microstructure modeling requires more effective approaches to capture the solidification physics for complex material systems. Property predictions require improved constitutive models based on better understanding of the governing deformation and failure mechanisms. Additionally, the multiphysics in the processes occur on different length and time scales and must be captured by different models. Better strategies should be developed to improve the accuracy and efficiency of data communication between different models.
- There is a significant opportunity to leverage data-driven modeling approaches to advance and accelerate the physics-driven predictions. One recent example by Herriott and Spear[40] demonstrates the use of deep learning to predict microstructure-sensitive mechanical properties of AM metals using 3D microstructural images as input. Once adequately trained, the deep-learning models are capable of predicting property maps like the one shown in Figure 9 in a matter of seconds. A recent review article by Kouraytem et al.[41] describes the similarities and distinctions between physics-driven and data-driven models for predicting P-M-P relationships in metal AM, emphasizing that the models are not mutually exclusive but can be used to inform one other.
- The computational costs for physic-based and data-based simulations can both be exceedingly high. To mitigate this, the community should better embrace the fast-

https://doi.org/10.1021/accountsmr.3c00108
Acc. Mater. Res. 2024, 5, 10−21

growing high-performance computing technologies (e.g., parallel computing, cloud computing, and GPU computing) and the efficient software libraries. In addition, the community can leverage the diverse resources and opportunities provided by some large-scale initiatives (such as the U.S. Department of Energy's High-Performance Computing for Manufacturing program).

- Continued efforts should focus on validating models. Round-robin style competitions, like the AM Modeling Challenge Series by AFRL and America makes and the AM Benchmark Challenges hosted by the National Institute of Standards and Technology, provide a substantial amount of data from well-controlled experiments. The data can help the community to identify gaps in modeling assumptions/formulations and to calibrate/validate the models. Additionally, because material properties can be highly sensitive to chemistry, temperature, and other conditions, future efforts should be invested to acquire and leverage data for condition-dependent material properties.

AUTHOR INFORMATION

Corresponding Authors

Wenda Tan − *Department of Mechanical Engineering, University of Michigan, Ann Arbor, Michigan 48109, United States;* orcid.org/0000-0002-5093-4990; Email: wendatan@umich.edu

Ashley Spear − *Department of Mechanical Engineering, University of Utah, Salt Lake City, Utah 84112, United States;* Email: ashley.spear@utah.edu

Complete contact information is available at: https://pubs.acs.org/10.1021/accountsmr.3c00108

Notes

The authors declare no competing financial interest.

Biographies

Wenda Tan is currently an assistant professor of Mechanical Engineering at the University of Michigan. He received his B.S. and M.S. degrees from Tsinghua University, China, and his Ph.D. degree from Purdue University, all in Mechanical Engineering. His major research interests include computational modeling and experimental characterization of advanced manufacturing technologies.

Ashley Spear is currently an associate professor of Mechanical Engineering at the University of Utah. She received her B.S. degree in Architectural Engineering from the University of Wyoming and her Ph.D. degree in Civil Engineering from Cornell University. Her major research interests are in the integration of advanced materials characterization, physics-based modeling, and data science to examine deformation, fatigue, and fracture in a wide range of materials.

ACKNOWLEDGMENTS

W.T. gratefully acknowledges Professors Lianyi Chen of the University of Wisconsin-Madison, Anthony Rollett of Carnegie Mellon University, Tao Sun of Northwestern University, and Dr. Alex Plotkowski of Oak Ridge National Laboratory for sharing their experimental results for the validation and calibration of his computational models. A.S. gratefully acknowledges Professor Anthony Rollett of Carnegie Mellon University and Dr. Ricardo Lebensohn of Los Alamos National Laboratory for helping her group to adopt the EVPFFT and MASSIF codes and for collaborating in the AFRL AM Modeling Challenge. Students and postdoctoral researchers responsible for carrying out the described work are effusively acknowledged: Xuxiao Li, Shardul Kamat, Carl Herriott, Carter Cocke, John Erickson, Dr. Nadia Kouraytem, and Dr. Aowabin Rahman. W.T. and A.S. gratefully acknowledge the support provided by the National Science Foundation under Grant No. CMMI-2119671.

REFERENCES

(1) Markl, M.; Körner, C. Multiscale Modeling of Powder Bed−Based Additive Manufacturing. *Annu. Rev. Mater. Res.* **2016**, *46*, 93−123.

(2) Wei, H. L.; Mukherjee, T.; Zhang, W.; Zuback, J. S.; Knapp, G. L.; De, A.; DebRoy, T. Mechanistic Models for Additive Manufacturing of Metallic Components. *Prog. Mater. Sci.* **2021**, *116*, 100703.

(3) Bayat, M.; Dong, W.; Thorborg, J.; To, A. C.; Hattel, J. H. A Review of Multi-Scale and Multi-Physics Simulations of Metal Additive Manufacturing Processes with Focus on Modeling Strategies. *Addit Manuf* **2021**, *47*, 102278.

(4) Tan, W.; Bailey, N. S.; Shin, Y. C. Investigation of Keyhole Plume and Molten Pool Based on a Three-Dimensional Dynamic Model with Sharp Interface Formulation. *J. Phys. D Appl. Phys.* **2013**, *46* (5), No. 055501.

(5) Tan, W.; Shin, Y. C. Analysis of Multi-Phase Interaction and Its Effects on Keyhole Dynamics with a Multi-Physics Numerical Model. *J. Phys. D Appl. Phys.* **2014**, *47* (34), 345501.

(6) Kouraytem, N.; Li, X.; Cunningham, R.; Zhao, C.; Parab, N.; Sun, T.; Rollett, A. D.; Spear, A. D.; Tan, W. Effect of Laser-Matter Interaction on Molten Pool Flow and Keyhole Dynamics. *Phys. Rev. Appl.* **2019**, *11* (6), No. 064054.

(7) Li, X.; Zhao, C.; Sun, T.; Tan, W. Revealing Transient Powder-Gas Interaction in Laser Powder Bed Fusion Process through Multi-Physics Modeling and High-Speed Synchrotron x-Ray Imaging. *Addit Manuf* **2020**, *35*, 101362.

(8) Li, X.; Guo, Q.; Chen, L.; Tan, W. Quantitative Investigation of Gas Flow, Powder-Gas Interaction, and Powder Behavior under Different Ambient Pressure Levels in Laser Powder Bed Fusion. *Int. J. Mach Tools Manuf* **2021**, *170*, 103797.

(9) Cunningham, R.; Zhao, C.; Parab, N.; Kantzos, C.; Pauza, J.; Fezzaa, K.; Sun, T.; Rollett, A. D. Keyhole Threshold and Morphology in Laser Melting Revealed by Ultrahigh-Speed x-Ray Imaging. *Science (1979)* **2019**, *363* (6429), 849−852.

(10) Kamat, S.; Li, X.; Stump, B.; Plotkowski, A.; Tan, W. Multi-Physics Modeling of Grain Growth during Solidification in Electron Beam Additive Manufacturing of Inconel 718. *Model Simul Mat Sci. Eng.* **2023**, *31* (1), No. 015002.

(11) Li, X.; Tan, W. Numerical Investigation of Effects of Nucleation Mechanisms on Grain Structure in Metal Additive Manufacturing. *Comput. Mater. Sci.* **2018**, *153*, 159−169.

(12) Kurz, W.; Giovanola, B.; Trivedi, R. Theory of Microstructural Development during Rapid Solidification. *Acta Metall.* **1986**, *34* (5), 823−830.

(13) Martin, J. H.; Yahata, B. D.; Hundley, J. M.; Mayer, J. A.; Schaedler, T. A.; Pollock, T. M. 3D Printing of High-Strength Aluminium Alloys. *Nature* **2017**, *549* (7672), 365−369.

(14) Pokharel, R.; Lind, J.; Kanjarla, A. K.; Lebensohn, R. A.; Li, S. F.; Kenesei, P.; Suter, R. M.; Rollett, A. D. Polycrystal Plasticity: Comparison between Grain-Scale Observations of Deformation and Simulations. *Annu. Rev. Condens. Matter Phys.* **2014**, *5* (1), 317−346.

(15) Francois, M. M.; Sun, A.; King, W. E.; Henson, N. J.; Tourret, D.; Bronkhorst, C. A.; Carlson, N. N.; Newman, C. K.; Haut, T.; Bakosi, J.; et al. Modeling of Additive Manufacturing Processes for Metals: Challenges and Opportunities. *Curr. Opin Solid State Mater. Sci.* **2017**, *21* (4), 198−206.

(16) Kok, Y.; Tan, X. P.; Wang, P.; Nai, M. L. S.; Loh, N. H.; Liu, E.; Tor, S. B. Anisotropy and Heterogeneity of Microstructure and Mechanical Properties in Metal Additive Manufacturing: A Critical Review. *Mater. Des* **2018**, *139*, 565−586.

(17) Gatsos, T.; Elsayed, K. A.; Zhai, Y.; Lados, D. A. Review on Computational Modeling of Process−Microstructure−Property Relationships in Metal Additive Manufacturing. *JOM* **2020**, *72* (1), 403−419.
(18) Vignesh, B.; Oliver, W. C.; Kumar, G. S.; Phani, P. S. Critical Assessment of High Speed Nanoindentation Mapping Technique and Data Deconvolution on Thermal Barrier Coatings. *Mater. Des* **2019**, *181*, 108084.
(19) Tari, V.; Lebensohn, R. A.; Pokharel, R.; Turner, T. J.; Shade, P. A.; Bernier, J. V.; Rollett, A. D. Validation of Micro-Mechanical FFT-Based Simulations Using High Energy Diffraction Microscopy on Ti-7Al. *Acta Mater.* **2018**, *154*, 273−283.
(20) Herriott, C.; Li, X.; Kouraytem, N.; Tari, V.; Tan, W.; Anglin, B.; Rollett, A. D.; Spear, A. D. A Multi-Scale, Multi-Physics Modeling Framework to Predict Spatial Variation of Properties in Additive-Manufactured Metals. *Model Simul Mat Sci. Eng.* **2019**, *27* (2), No. 025009.
(21) Lebensohn, R. A.; Kanjarla, A. K.; Eisenlohr, P. An Elasto-Viscoplastic Formulation Based on Fast Fourier Transforms for the Prediction of Micromechanical Fields in Polycrystalline Materials. *Int. J. Plast* **2012**, *32*, 59−69.
(22) Bartlett, J. L.; Li, X. An Overview of Residual Stresses in Metal Powder Bed Fusion. *Addit Manuf* **2019**, *27*, 131−149.
(23) Cocke, C. K.; Rollett, A. D.; Lebensohn, R. A.; Spear, A. D. The AFRL Additive Manufacturing Modeling Challenge: Predicting Micromechanical Fields in AM IN625 Using an FFT-Based Method with Direct Input from a 3D Microstructural Image. *Integr Mater. Manuf Innov* **2021**, *10* (2), 157−176.
(24) Chapman, M. G.; Shah, M. N.; Donegan, S. P.; Scott, J. M.; Shade, P. A.; Menasche, D.; Uchic, M. D. AFRL Additive Manufacturing Modeling Series: Challenge 4, 3D Reconstruction of an IN625 High-Energy Diffraction Microscopy Sample Using Multi-Modal Serial Sectioning. *Integr Mater. Manuf Innov* **2021**, *10*, 129−141.
(25) Menasche, D. B.; Musinski, W. D.; Obstalecki, M.; Shah, M. N.; Donegan, S. P.; Bernier, J. V.; Kenesei, P.; Park, J.-S.; Shade, P. A. AFRL Additive Manufacturing Modeling Series: Challenge 4, in Situ Mechanical Test of an IN625 Sample with Concurrent High-Energy Diffraction Microscopy Characterization. *Integr Mater. Manuf Innov* **2021**, *10* (3), 338−347.
(26) Suter, R. M.; Hennessy, D.; Xiao, C.; Lienert, U. Forward Modeling Method for Microstructure Reconstruction Using X-Ray Diffraction Microscopy: Single-Crystal Verification. *Review of scientific instruments* **2006**, *77* (12), 123905.
(27) Bernier, J. V.; Barton, N. R.; Lienert, U.; Miller, M. P. Far-Field High-Energy Diffraction Microscopy: A Tool for Intergranular Orientation and Strain Analysis. *J. Strain Anal Eng. Des* **2011**, *46* (7), 527−547.
(28) Lienert, U.; Li, S. F.; Hefferan, C. M.; Lind, J.; Suter, R. M.; Bernier, J. V.; Barton, N. R.; Brandes, M. C.; Mills, M. J.; Miller, M. P.; et al. High-Energy Diffraction Microscopy at the Advanced Photon Source. *Jom* **2011**, *63*, 70−77.
(29) Pokharel, R. Overview of High-Energy x-Ray Diffraction Microscopy (HEDM) for Mesoscale Material Characterization in Three-Dimensions. In *Materials Discovery and Design: By Means of Data Science and Optimal Learning*; Springer, 2018; pp 167−201.
(30) Pokharel, R.; Lebensohn, R. A. Instantiation of Crystal Plasticity Simulations for Micromechanical Modelling with Direct Input from Microstructural Data Collected at Light Sources. *Scr Mater.* **2017**, *132*, 73−77.
(31) Eshelby, J. D. The Determination of the Elastic Field of an Ellipsoidal Inclusion, and Related Problems. *Proc. R Soc. Lond A Math Phys. Sci.* **1957**, *241* (1226), 376−396.
(32) Groeber, M. A.; Jackson, M. A. DREAM. 3D: A Digital Representation Environment for the Analysis of Microstructure in 3D. *Integr Mater. Manuf Innov* **2014**, *3*, 56−72.
(33) Sola, A.; Nouri, A. Microstructural Porosity in Additive Manufacturing: The Formation and Detection of Pores in Metal Parts Fabricated by Powder Bed Fusion. *J. Adv. Manuf Process* **2019**, *1* (3), e10021.
(34) Du Plessis, A.; Yadroitsava, I.; Yadroitsev, I. Effects of Defects on Mechanical Properties in Metal Additive Manufacturing: A Review Focusing on X-Ray Tomography Insights. *Mater. Des* **2020**, *187*, 108385.
(35) Erickson, J. M.; Rahman, A.; Spear, A. D. A Void Descriptor Function to Uniquely Characterize Pore Networks and Predict Ductile-Metal Failure Properties. *Int. J. Fract.* **2020**, *225*, 47−67.
(36) Boyce, B. L.; Salzbrenner, B. C.; Rodelas, J. M.; Swiler, L. P.; Madison, J. D.; Jared, B. H.; Shen, Y. Extreme-value Statistics Reveal Rare Failure-critical Defects in Additive Manufacturing. *Adv. Eng. Mater.* **2017**, *19* (8), 1700102.
(37) Kramer, S. L. B.; Jones, A.; Mostafa, A.; Ravaji, B.; Tancogne-Dejean, T.; Roth, C. C.; Bandpay, M. G.; Pack, K.; Foster, J. T.; Behzadinasab, M.; et al. The Third Sandia Fracture Challenge: Predictions of Ductile Fracture in Additively Manufactured Metal. *Int. J. Fract.* **2019**, *218*, 5−61.
(38) Spear, A. D.; Czabaj, M. W.; Newell, P.; DeMille, K.; Phung, B. R.; Zhao, D.; Creveling, P.; Briggs, N.; Brodbine, E.; Creveling, C.; et al. The Third Sandia Fracture Challenge: From Theory to Practice in a Classroom Setting. *Int. J. Fract.* **2019**, *218*, 171−194.
(39) Watring, D. S.; Benzing, J. T.; Kafka, O. L.; Liew, L.-A.; Moser, N. H.; Erickson, J.; Hrabe, N.; Spear, A. D. Evaluation of a Modified Void Descriptor Function to Uniquely Characterize Pore Networks and Predict Fracture-Related Properties in Additively Manufactured Metals. *Acta Mater.* **2022**, *223*, 117464.
(40) Herriott, C.; Spear, A. D. Predicting Microstructure-Dependent Mechanical Properties in Additively Manufactured Metals with Machine-and Deep-Learning Methods. *Comput. Mater. Sci.* **2020**, *175*, 109599.
(41) Kouraytem, N.; Li, X.; Tan, W.; Kappes, B.; Spear, A. D. Modeling Process−Structure−Property Relationships in Metal Additive Manufacturing: A Review on Physics-Driven versus Data-Driven Approaches. *Journal of Physics: Materials* **2021**, *4* (3), No. 032002.

https://doi.org/10.1021/accountsmr.3c00108
Acc. Mater. Res. 2024, 5, 10−21